3

GEOMETRY, DILUTION AND COMPOSITION OF SINGLE-BEAD DEPOSITS

3.1 INTRODUCTION

The first phase of experiments involved single-bead deposits. It was intended that these experiments would reveal the major influences on the geometry and composition of single beads. The chapter commences with a description of the experimental procedure, and each subsequent section focuses on the factors affecting a particular feature of the deposit. For single-bead deposits, the features of major interest are the bead width, penetration, height, dilution and composition. Throughout, down-hand deposition is used, as this is the preferred mode of operation in industry.

3.2 EXPERIMENTAL TECHNIQUE

Two welding consumables were used for the single-bead experiments. The first, consumable A, was a 2.4mm diameter chromium-carbide-type alloy-cored electrode. The second, consumable B, was also a chromium-carbide-type electrode, but 2.8mm in diameter. Both of these consumables were found to produce single-bead deposits with predominantly austenitic matrices. The approximate compositions of both consumables are listed in Table 3.1. The concentrations of carbon and sulphur were obtained from combustion carbon and sulphur analyses whereas the concentrations of all other elements were obtained using optical emission spectroscopy.

Consumable	*Cr*	*C*	*Mn*	*Ni*	*Si*	*B*	*S*	*Fe*
A	*25.1*	*6.55*	*1.2*	*0.3*	*0.6*	*0.2*	*0.02*	*bal.*
B	*26.7*	*5.93*	*0.4*	*0.2*	*0.9*	*-*	*0.02*	*bal.*

Table 3.1: - The approximate compositions of the consumables used in the current work. All concentrations are given in wt.%.

3.2.1 Experimental Program for Consumable A.

Sixty-four single beads 150mm long were deposited on to mild steel substrates 10mm thick, 200mm long and 50mm wide. In each case a 100mm long run-on plate was used. The power supply was a DC transformer-rectifier type with a 400 A capacity at 100% duty cycle. The power supply was connected to a wire feeder that fed the consumable through a water-cooled cable and gun. The gun was fixed and the steel plate sample was translated underneath it on a motorised X-Y table with a calibrated speed controller.

The experimental design comprised four travel speed settings, (150, 250, 350 and 450mm/min), four voltage settings (25, 28, 31 and 34V) and four current settings (250, 300, 350 and 400A). The work distance was 40mm and the polarity was direct-current, electrode-positive (DCEP). Although no information was provided regarding appropriate settings for travel speed, the welding currents and voltages were selected in such a way that they spanned the range recommended by the manufacturer.

The welding current and voltage were set on test pieces of steel prior to each experiment. Voltages were measured between the work piece and the contact tip, not at the wire feed unit. A CSIRO welding monitor (Dick, 1991) was used to display instantaneous values

for welding current and voltage and to log the data for each run. The monitor takes 5000 measurements of these parameters for each second of the welding run. It then averages these and displays one value per second of operation.

In addition, a further 8 single beads were deposited to investigate preheat temperatures to 300^{o}C and work distances ranging between 30 and 60mm. Sixteen samples were also repeated using direct-current, electrode-negative (DCEN) polarity for comparison.

3.2.2 Experimental Program for Consumable B

Fifteen single beads 250mm long were deposited on to mild steel substrates 25mm thick, 50mm wide and 350mm long. Voltages ranged from 25 to 31V, currents from 200 to 400A and travel speeds from 400 to 800mm/min. In these experiments the work distances were also varied from 15 to 40mm. DCEP polarity was used in all cases.

3.2.3 Analysis of Samples for Consumable A

Three slices were cut from each sample. Each slice was approximately 10mm in thickness. One face of each slice was surface ground and etched with 5% Nital. The prepared section was then placed on an optical projector with a 10:1 magnification ratio and the bead profile was traced on to high quality tracing paper. This traced profile was then transferred to a digitiser pad where cross-sectional areas and hence dilutions were determined. Other parameters were also measured, including bead width, penetration and height.

3.2.4 Analysis of Samples for Consumable B

The height and width of each bead were measured using digital vernier callipers.

3.3 THE EFFECTS OF WELDING PARAMETERS ON BEAD WIDTH

3.3.1 A First-Principles Approach

The theoretical analysis of Christensen *et al.* (1965) proves to be a useful tool in estimating the width of a deposit. This work derived non-dimensional solutions for bead width and other parameters of interest in terms of a dimensionless operating parameter, *n*, given by:

$$n = \varsigma_a \frac{V_a I S}{4\pi\alpha k (T_c - T_o)} \quad \cdots\cdots\cdots (3.1)$$

where:

η_a = arc efficiency,
V_a = arc voltage,
I = welding current,
S = travel speed,
α = thermal diffusivity of the base material,
k = thermal conductivity of the base material,
T_c = chosen reference temperature, and
T_o = initial substrate temperature.

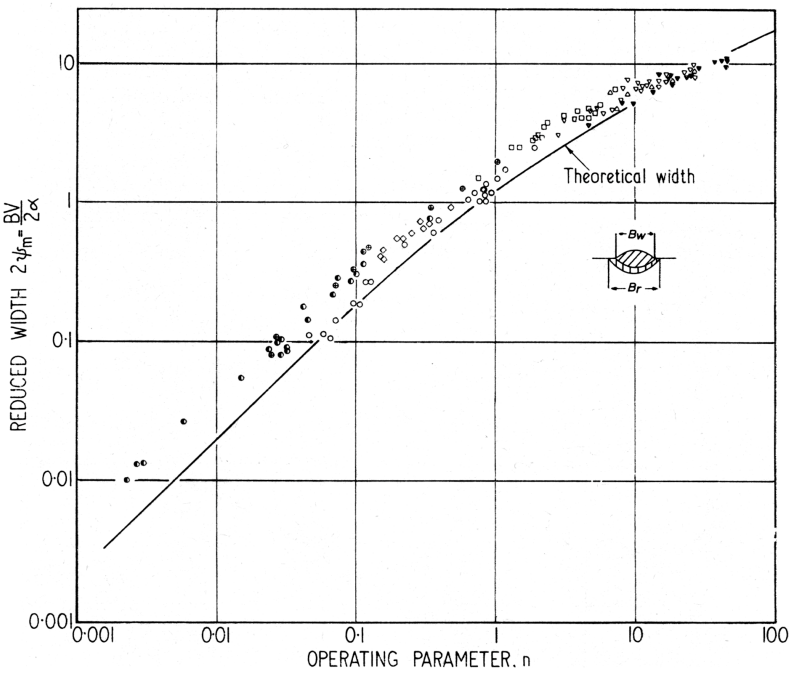

Figure 3.1: - The analytical solution for bead width proposed by Christensen *et al.* (1965).

The chosen reference temperature can be taken to be the melting point for the substrate material in order to predict the fusion line position and hence the bead width. If the thermal properties are assumed to remain constant then, for a given material, the value of n is determined by the arc voltage, current and travel speed.

Christensen's non-dimensional solution for bead width is a complicated and implicit function in n. However, although there were discrepancies, the solution was found to achieve reasonable agreement with experiment over a range of n values spanning four orders of magnitude. Open-arc hardfacing occurs over a much smaller range of n values. A lower limit for n in open-arc hardfacing may correspond to the condition where:

V_a = 24V,
I = 200A, and
S = 300mm/min.

An upper limit may correspond to:

V_a = 34V,
I = 400A, and
S = 900mm/min.

If the arc efficiency is assumed to remain relatively constant and representative thermal property values are available, it is possible to estimate the range of n values over which open-arc hardfacing occurs. The above-mentioned conditions would result in the lower limit for n being approximately 5 and the upper limit being approximately 50.

The form of Christensen's solution for bead width is:

$$\frac{wS}{2\alpha} = F(n) \quad \cdots\cdots\cdots (3.2)$$

where w is the bead width and $F()$ denotes a function.

If the substrate material is mild steel then, for the range of n values corresponding to open-arc hardfacing, equation 3.2 may be approximately represented by the following expression:

$$\frac{wS}{2\acute{a}\square} = a_1 + a_2 n \quad \cdots\cdots\cdots \quad (3.3)$$

where a_1 and a_2 are constant coefficients.

Now, n is given by equation 3.1. For a given combination of substrate material and welding consumable the only variables that change are the arc voltage, V_a, current, I, and travel speed, S. Thus substituting equation 3.1 into 3.3 and combining constant terms provides the following expression for the bead width, with C_1 and C_2 being constants.

$$w = \frac{C_1}{S} + C_2 V_a I$$

Christensen's analysis suggests that it is the arc voltage, not the contact tip-to-work voltage, that is responsible for generating the heat that is transferred to the weld pool. In the case of the consumable electrode processes this may not be strictly correct. The voltage drop along the welding wire, between the contact tip and the arc, preheats the electrode and increases its enthalpy. This increased enthalpy is then added to the weld pool as the globules are transferred across the arc zone. Thus it would seem reasonable, for flux-cored arc welding, to use the contact tip-to-work voltage in place of the arc voltage, so that:

$$w = \frac{C_1}{S} + C_2 V I \cdots\cdots\cdots (3.4)$$

Even though the substitution of contact tip-to-work voltage for arc voltage seems reasonable, it is essentially an adjustment of convenience. The contact tip-to-work voltage is a much easier parameter to measure (and set) than the arc voltage. It is important to note, however, that adapting Christensen's solution to open-arc hardfacing is not likely to predict the resulting bead widths directly from first principles. The intention was to use their first-principles analysis as a starting point and adapt it to arrive at an expression that has an appropriate form.

The theory developed by Christensen *et al.* suggests that the values of C_1 and C_2 are dependent only on the thermal properties of the substrate material. However, in reality the deposition characteristics of the welding consumable will play a role, as they affect the deposition rate and hence the rate at which the enthalpy associated with metal transfer is added to the weld pool. Least-squares best-fit values for C_1 and C_2 were obtained for both consumables used in the current work. Figure 3.2 shows the measured bead widths plotted against fitted bead widths for consumable A. Figure 3.3 shows a similar fit for consumable B. It can be seen that good fits have been achieved for both welding consumables and that equation 3.4 appears to provide a form of expression suitable for describing bead widths for single beads-on-plate.

The agreement between fitted and measured bead widths appears to be good for all beads except those with widths greater than 20mm (see Figure 3.2). Thus one might expect equation 3.4 to accurately describe bead width data for beads produced under conditions that involve moderate-to-high travel speeds. These conditions generally result in a lower bead width, and a bead profile similar to that shown in Figure 3.4(a). Conversely, wide beads are produced under conditions where the deposition rates are

high and the travel speeds are low, and an example of such a condition is shown in Figure 3.4(b). As the weld pool rolls over unmelted substrate there will be heat transfer from the weld pool to the adjacent solid material. This heat transfer is likely to cause additional melting and result in the bead being wider than equation 3.4 might predict. Another issue also arises, however, in that the beads were deposited on 10mm thick substrates. It is therefore possible that, at low speeds and high heat inputs, there was appreciable bulk heating of the steel bars ahead of the welding arc. Such heating would also contribute to increases in bead width.

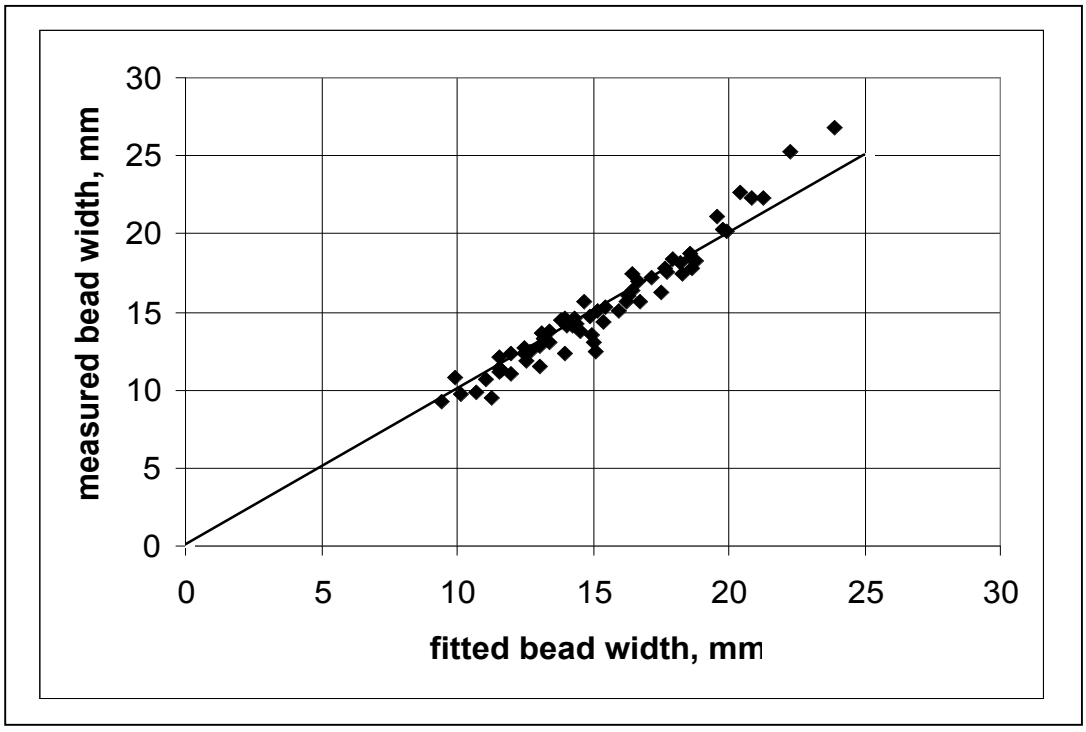

Figure 3.2: - Measured bead width vs the least-squares best fit to equation 3.4 for 64 samples deposited with consumable A (2.4mm diameter).

The form of equation 3.4 implies that the bead width will asymptote to a specific non-zero value as the travel speed is increased. However, this may not necessarily be the case. It must be remembered that equation 3.4 is a first order fit to Christensen's

solution over the range of *n* values encountered in open-arc hardfacing. It will, however, provide accurate predictions for most practical welding conditions.

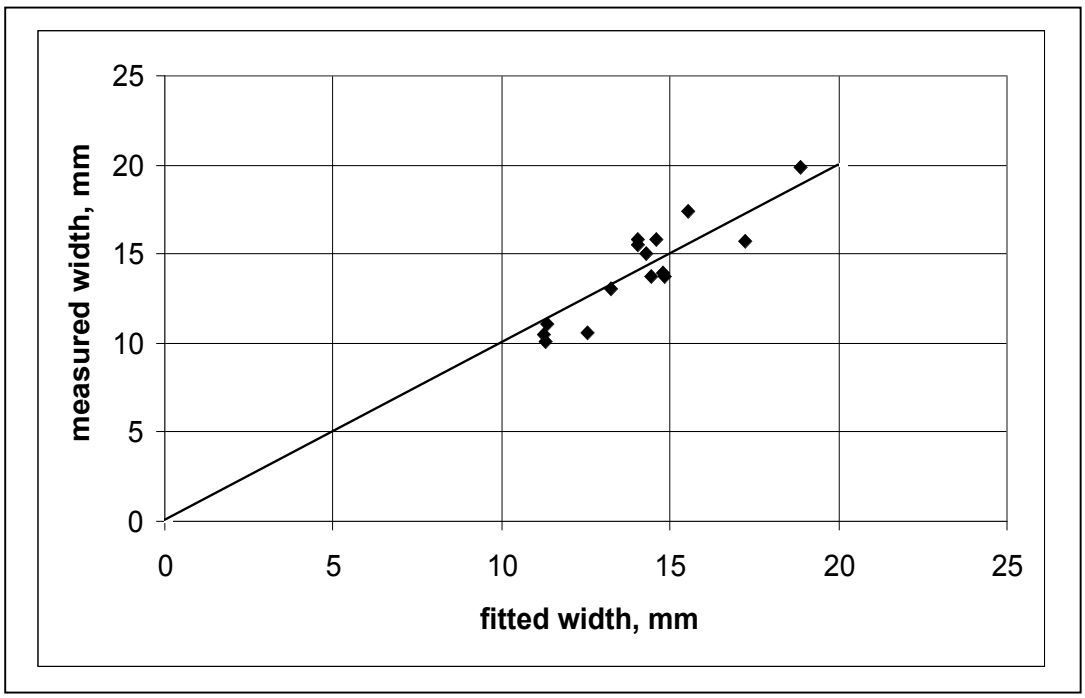

Figure 3.3: - Measured bead width vs the least-squares best fit to equation 3.4 for the 15 samples deposited with consumable B (2.8mm diameter).

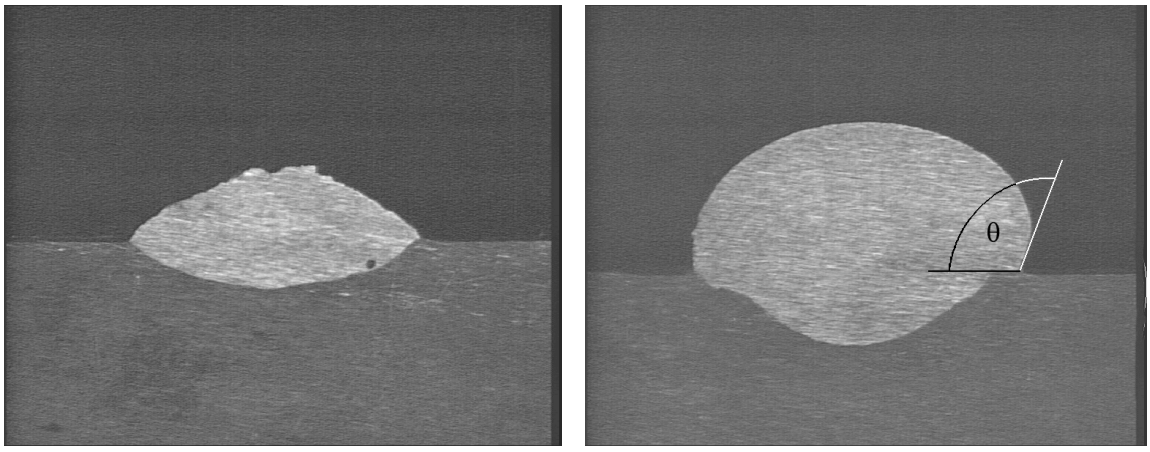

(a) 34V, 250A and 450mm/min (b) 28V, 350A and 250mm/min

Figures 3.4: - An example of the bead profiles that result at moderate-to-high travel speeds is shown in (a). If the deposition rate is high and the travel speed is low, a profile such as that shown in (b) will result. In this case there is a tendency for the weld pool to roll over unmelted substrate and the value of θ will be greater than 90°.

3.3.2 The Effects of Work Distance and Preheat Temperature

Equation 3.4 relates the bead width to the welding voltage, current and travel speed. However, the extent to which the work distance and preheat temperature affect the bead width is not revealed. The variation of bead width with work distance is plotted in Figure 3.5 and the variation with preheat temperature is plotted in Figure 3.6. It can be seen that the bead width is not particularly sensitive to work distance. Increasing the preheat temperature to 300°C does, however, lead to a somewhat greater quantity of substrate being melted and hence a slightly greater bead width.

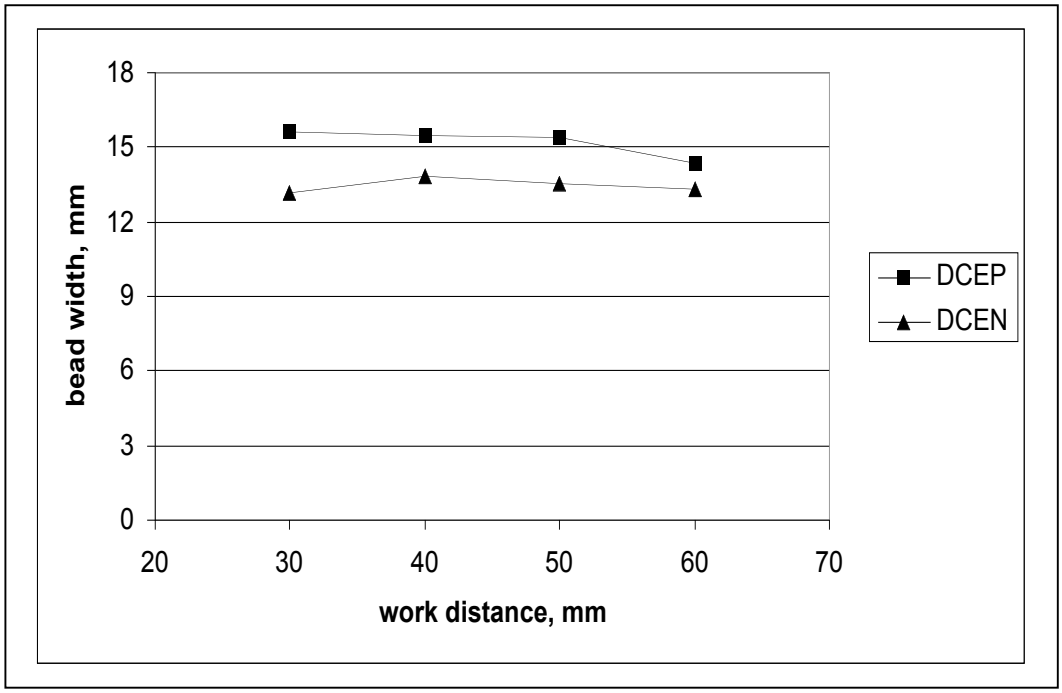

Figure 3.5: - The effect of work distance on the bead width. These samples were deposited with consumable A and the base welding conditions were 31V, 300A, 350mm/min with no preheat.

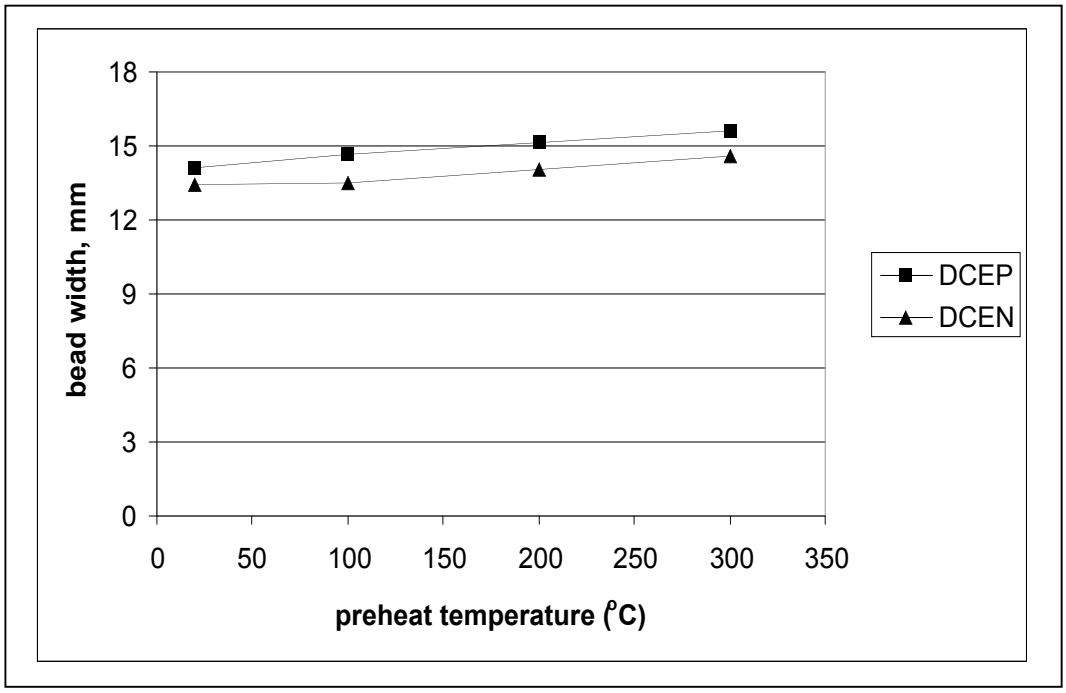

Figure 3.6: - The effect of preheat temperature on the bead width. These samples were deposited with consumable A and the base welding conditions were 31V, 300A, 350mm/min and a 40mm work distance.

3.4 THE EFFECTS OF WELDING PARAMETERS ON PENETRATION

3.4.1 Expressions for Penetration

It is possible to adapt Christensen's model and arrive at an expression for penetration in the same way as it was for bead width:

$$2p = \frac{C_1}{S} + C_2 VI \quad \cdots\cdots\cdots (3.5)$$

Christensen's model predicts that the fusion line will be a semi-circle in the case where a single bead is deposited on a thick plate. If the fusion lines of single-bead deposits were semi-circular, the values of C_1 and C_2 in equation 3.5 would be the same as the values

they assumed in equation 3.4 for bead width. The data for Consumable A have been fitted to equation 3.5 and are plotted in Figure 3.7. The measured data are plotted against values from the least-squares best fit.

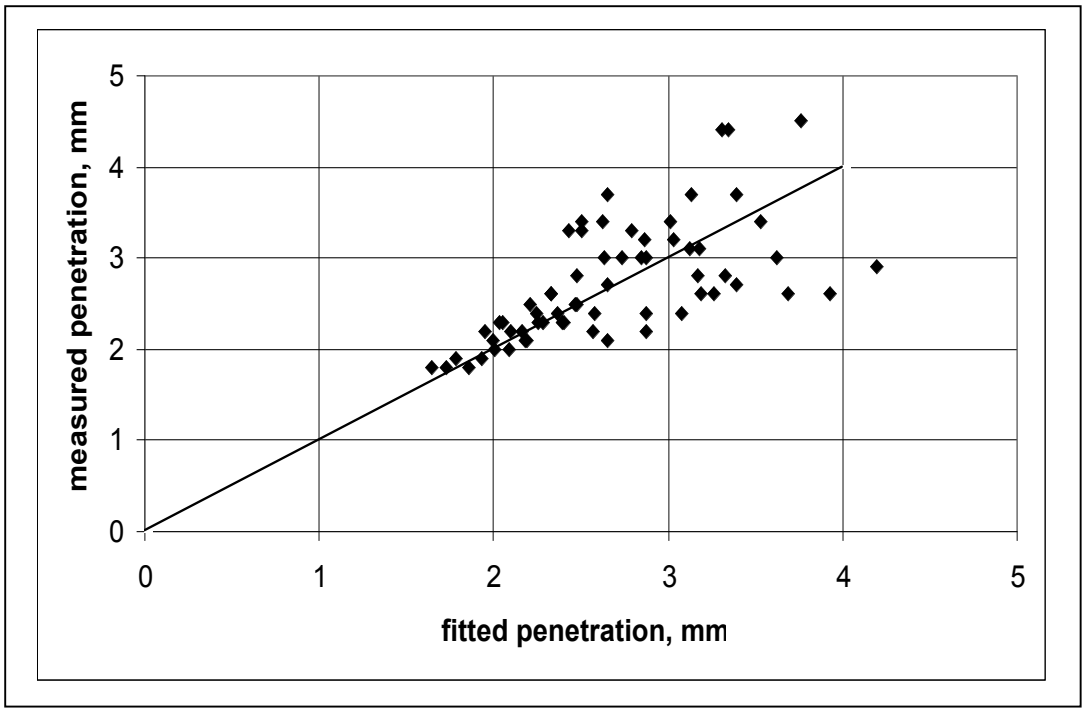

Figure 3.7: - Measured penetration against fitted penetration for consumable A (2.4mm diameter). The data are a least-squares best fit to equation 3.5.

It can be seen that the fit for penetration is poor. There are certain influences on penetration that are not accounted for by the Christensen model. It was seen in section 2.3 that weld pool convection, weld pool depression and the molten droplets play significant roles in determining the shape of the weld pool and hence the penetration. It appears from the plot that an adaption of Christensen's model will provide accurate predictions at low penetrations, but as the arc voltage and current rise the above-mentioned effects become increasingly significant. An empirical term was added to equation 3.5 in an attempt to improve the fit and account for these effects but this attempt met with limited success.

Jackson and Shrubsall (1953) used an empirical approach, attributed to Gunnert, for estimating weld bead penetrations (see section 2.3.6.1). They proposed that penetration data would take the following form:

$$p = K \sqrt[3]{\frac{I^4}{S V^2}} \quad \cdots\cdots\cdots (2.6) \quad \text{(page 22)}$$

where K is a fitted constant term.

Kim, Basu and Siores (1994) fitted their penetration data to an expression of the form:

$$p = 10^{a_1} d^{a_2} G^{a_3} I^{a_4} V^{a_5} \quad \cdots\cdots\cdots (3.6)$$

The data were obtained from gas-metal-arc weld deposits. In equation 3.6, d is the consumable diameter, G is the gas flow rate and a_1, a_2, a_3, a_4, a_5 are fitted constants. In open-arc hardfacing there is no gas flow rate as such, as the electrodes are self-shielding. The travel speed will also play a role in determining the weld bead penetration, but was not included in the expression. A more appropriate form of expression is:

$$p = b_1 V^{b_2} I^{b_3} S^{b_4} \quad \cdots\cdots\cdots (3.7)$$

where b_1, b_2, b_3, b_4 are fitted constants. The penetration data for consumable A were fitted to both expressions 2.6 and 3.7. The fit achieved with equation 3.7 (shown in Figure 3.8) was slightly better than that achieved with equation 2.6. It can be seen that the fit is also better than that achieved with the adapted form of Christensen's model, but that there is still significant spread. The fitted equation is:

$$p = 10^{-4.47} V^{-0.55} I^{0.81} S^{-0.30} \quad \cdots\cdots\cdots (3.8)$$

If the fit for equation 2.6 is expressed in the same form as equation 3.8 it becomes:

$$p = 10^{-5.66} V^{-0.67} I^{1.33} S^{-0.33} \quad \cdots\cdots\cdots (3.9)$$

There are similarities between equations 3.8 and 3.9. Both suggest welding current is the dominant influence on penetration. As the current increases so too does the penetration. Both equations also display close agreement regarding the sensitivity of penetration to arc voltage and travel speed. However, none of the above mentioned equations demonstrate an ability to describe penetration accurately. At best, equation 2.6 can be used as a guide to the relative sensitivities of penetration to each parameter. This equation achieved a fit that was comparable to those of equations 3.5 and 3.7, yet it only requires one constant value to be established. In addition, it has been found useful in estimating submerged-arc weld bead penetrations (Jackson and Shrubsall, 1953).

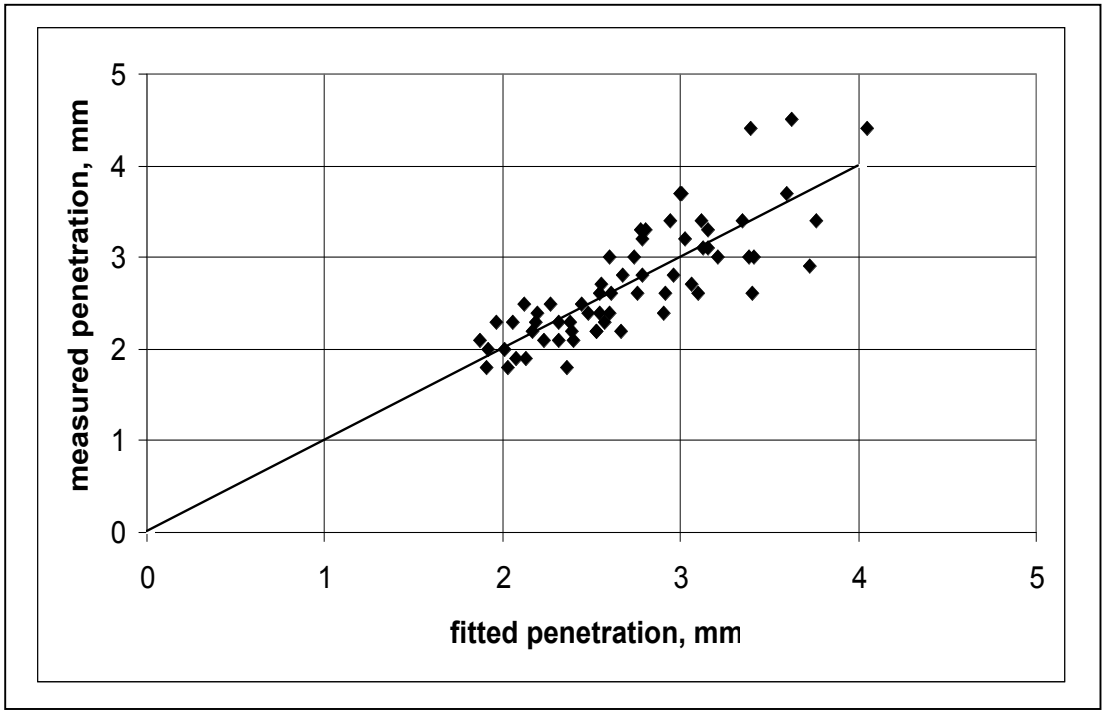

Figure 3.8: - Measured penetrations vs fitted penetrations for consumable A (2.4mm diameter). The fitted penetrations are a least-squares best fit to equation 3.7.

3.4.2 The Effects of Work Distance and Preheat Temperature

The effects of work distance and preheat temperature are shown in Figures 3.9 and 3.10 respectively. It can be seen that there is a significant drop in penetration as the work distance is increased. Kim and Na (1995) proposed that this effect is related to the increase in arc length that occurs when the work distance is increased. These workers suggested that longer arcs cause the distributions of heat, arc pressure and current flux to be expanded, resulting in less penetration. By comparison, there does not appear to be a clear trend in Figure 3.10. This is somewhat unexpected as one might anticipate a trend towards increasing penetration with increasing preheat temperature. As the preheat temperature increases, a greater amount of substrate material will melt. Figure 3.6 showed that increases in preheat temperatures resulted in wider beads, but it appears that higher preheat temperatures may be required before the effect on penetration becomes obvious.

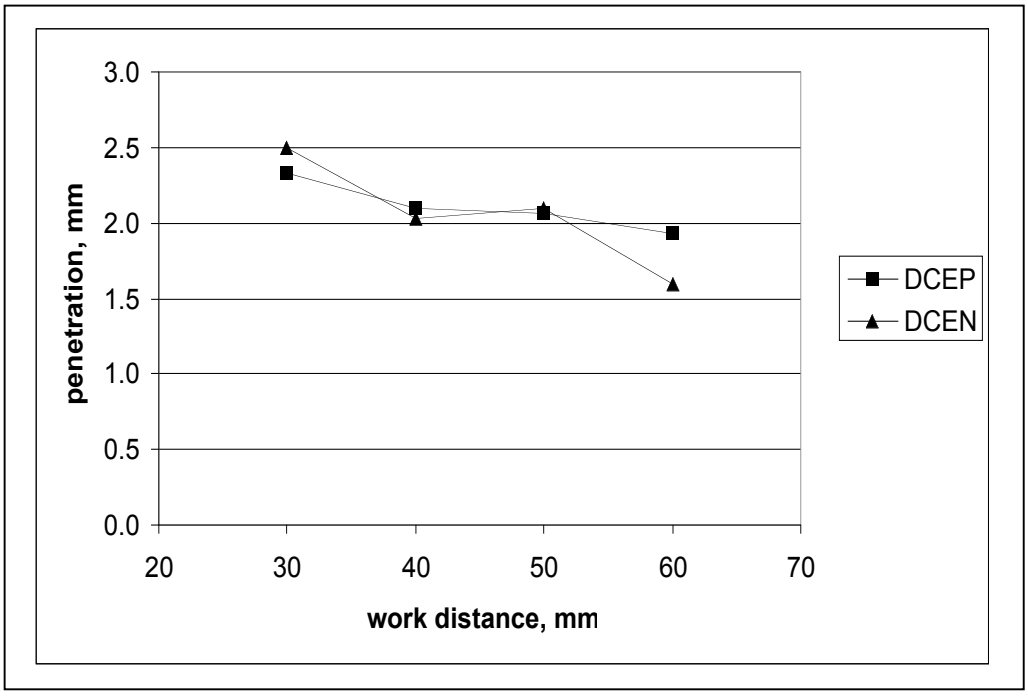

Figure 3.9: - The variation in penetration with work distance. All data points were obtained with consumable A and the base welding conditions were 31V, 300A, 350mm/min and no preheat.

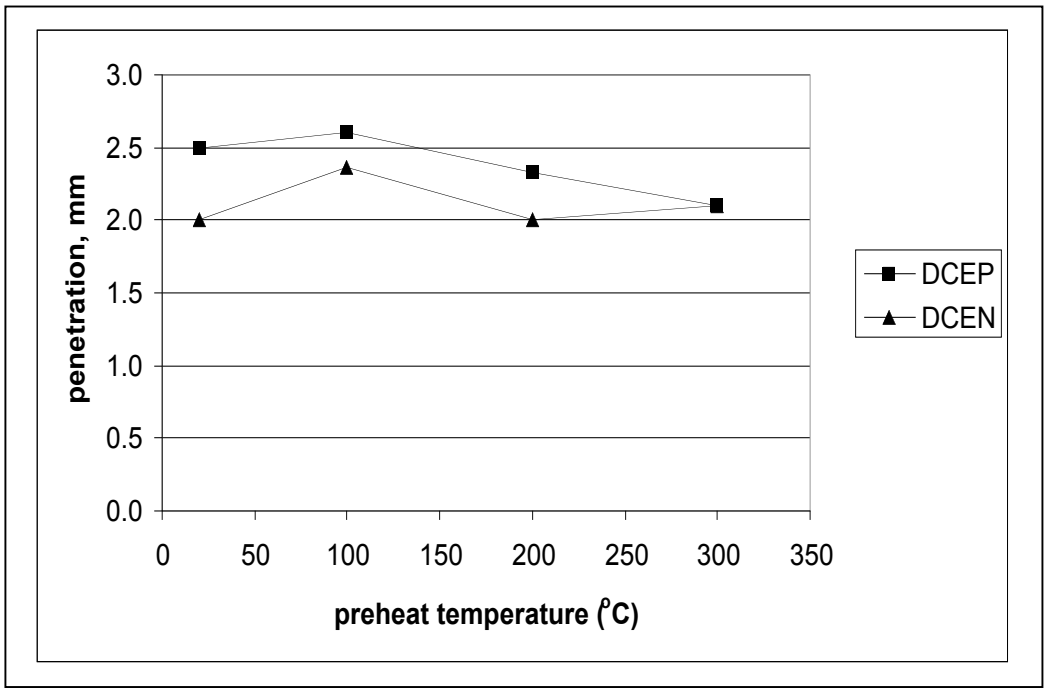

Figure 3.10: - The variation in penetration with preheat temperature. All data points were obtained with consumable A and the base welding conditions were 31V, 300A, 40mm, 350mm/min and no preheat.

3.5 BEAD HEIGHT

3.5.1 An Expression for Bead Height

It was seen in the literature review that little has been published regarding the prediction of bead height directly from the selected welding parameters. Consequently, an approach is outlined here. The approach is based on the assumption that the profile of a bead can be modelled by a parabolic function. This is a reasonable assumption, particularly at moderate-to-high welding speeds. An example of a bead profile that resembles a parabola was given in Figure 3.4(a), where the travel speed was 450mm/min. A schematic representation of the proposed model is given in Figure 3.11.

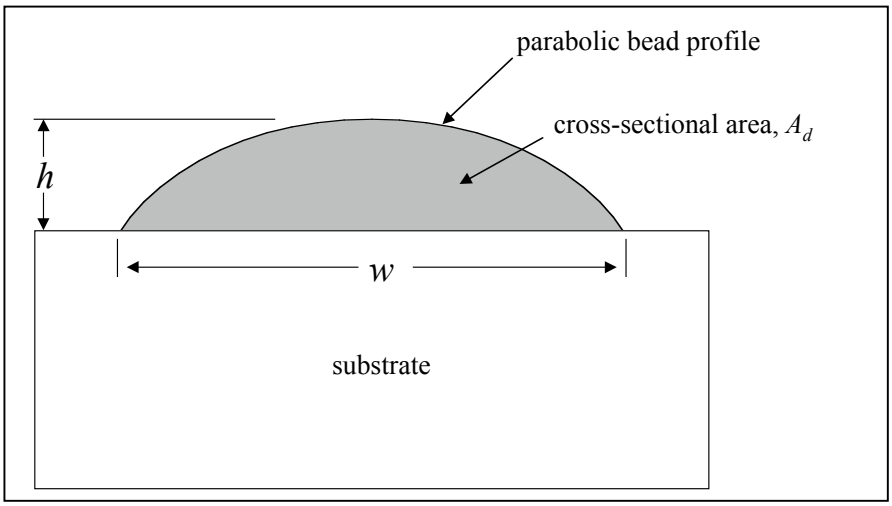

Figure 3.11: - A schematic representation of the parabolic model for a single-bead deposit.

The principle of conservation of mass requires that the area under the parabola is equal to the cross-sectional area of deposited material, A_d. It can be shown by integration that the area under the curve is equal to two thirds of the product of the width, w, and the height, h. It can also be shown that the cross-sectional area of deposited material is equal to the deposition rate divided by the product of density and travel speed, *i.e.*:

$$A_d = \frac{2}{3} hw = \frac{W}{\rho S} \quad \cdots\cdots\cdots (3.10)$$

where h = the peak height of the parabolic function, (bead height)
w = the width of the parabolic function, (bead width)
W = deposition rate,
ρ = density of an all-weld-metal deposit, and
S = travel speed.

It is possible to obtain h explicitly from equation 3.10:

$$h = \frac{3}{2} \frac{W}{\rho S w} \quad \cdots\cdots\cdots (3.11)$$

This expression for bead height is compared with data from three different welding consumables in Figure 3.12. (Data for the third welding consumable, consumable C, are reproduced by kind permission of Mr. B.K. Arnold of CSIRO Manufacturing Science and Technology. Consumable C was 2.8mm in diameter and had a similar composition to consumables A and B.) Values for w were obtained from measured bead widths and values for W were obtained from measured deposition rates.

It can be seen that if the predicted bead height is 4mm or less one can be confident that the prediction is accurate. This will most likely be the case if the welding condition involves a moderate-to-high travel speed. However, as the height of the beads increases so too do the discrepancies and, if the predicted bead height is greater than 4mm, the error may be large. Large errors are particularly likely if the deposition rate is high and the travel speed is low.

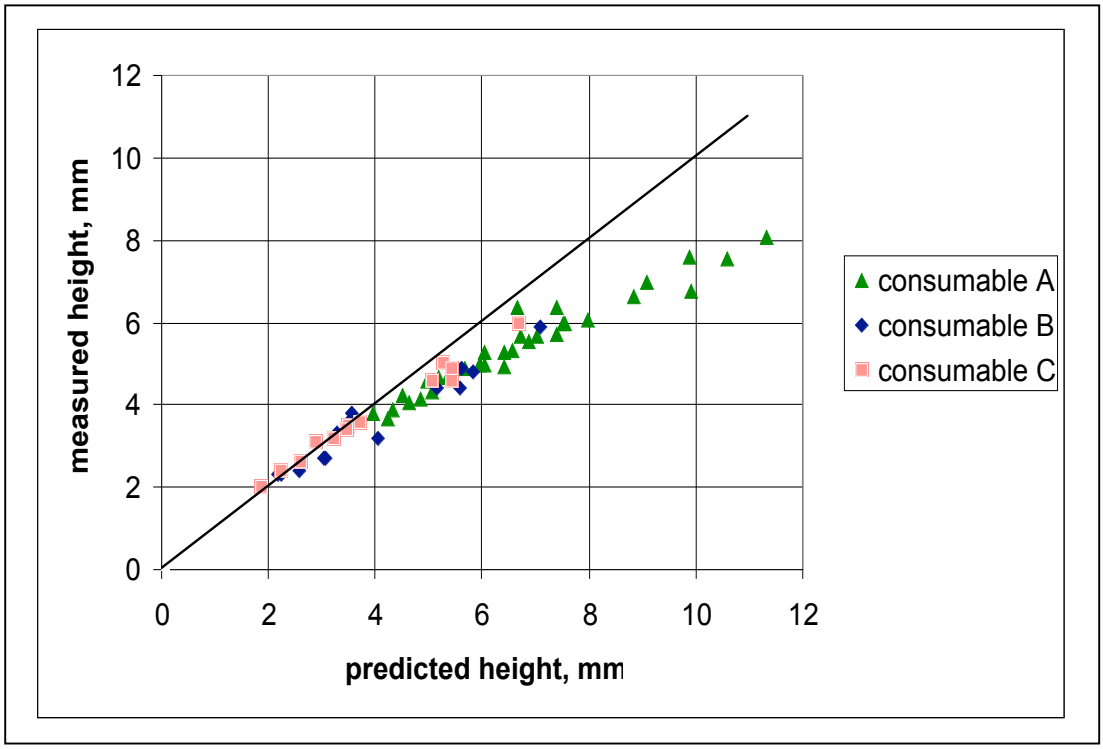

Figure 3.12: - A plot of measured heights for three different welding consumables against the height predicted by equation 3.11. All samples were deposited with DCEP polarity.

The discrepancies between equation 3.11 and measured values are caused by gravity-induced flow of the weld pool. Such flow has occurred in the case of the weld bead shown in Figure 3.4(b). It can be seen that in this case the weld pool has, to some extent, flowed over unmelted substrate. The bead profile deviates significantly from a parabolic profile when gravity-induced flow occurs and consequently the predictions made by equation 3.11 become increasingly inaccurate. Gravity-induced flow occurs to a greater extent as the height of the weld pool increases.

Fortunately, there is a strong correlation between the heights predicted by equation 3.11 and those measured in practice. The nature of the correlation is such that equation 3.11 is amenable to an empirical correction that accounts for this gravity-induced flow. An empirical correction has been included in equation 3.12:

$$h = \frac{3}{2}\frac{W}{\tilde{n}Sw} - 84.4\left(\frac{3}{2}\frac{W}{\tilde{n}Sw}\right)^{2.25} \qquad \{h - 8\times10^{-3}\ \mathrm{m}\} \quad \cdots\cdots(3.12)$$

The height measurements from the three different welding consumables are plotted against the fitted values for equation 3.12 in Figure 3.13.

Equation 3.12 is likely to accurately predict the bead height for many high chromium, high carbon type deposits, as their tendency to flow will be similar. Different consumable types are also likely to fit to an expression of the same form as equation 3.12. However, it is anticipated that the constant and index in the empirical correction term will change as the tendency to flow changes from material to material.

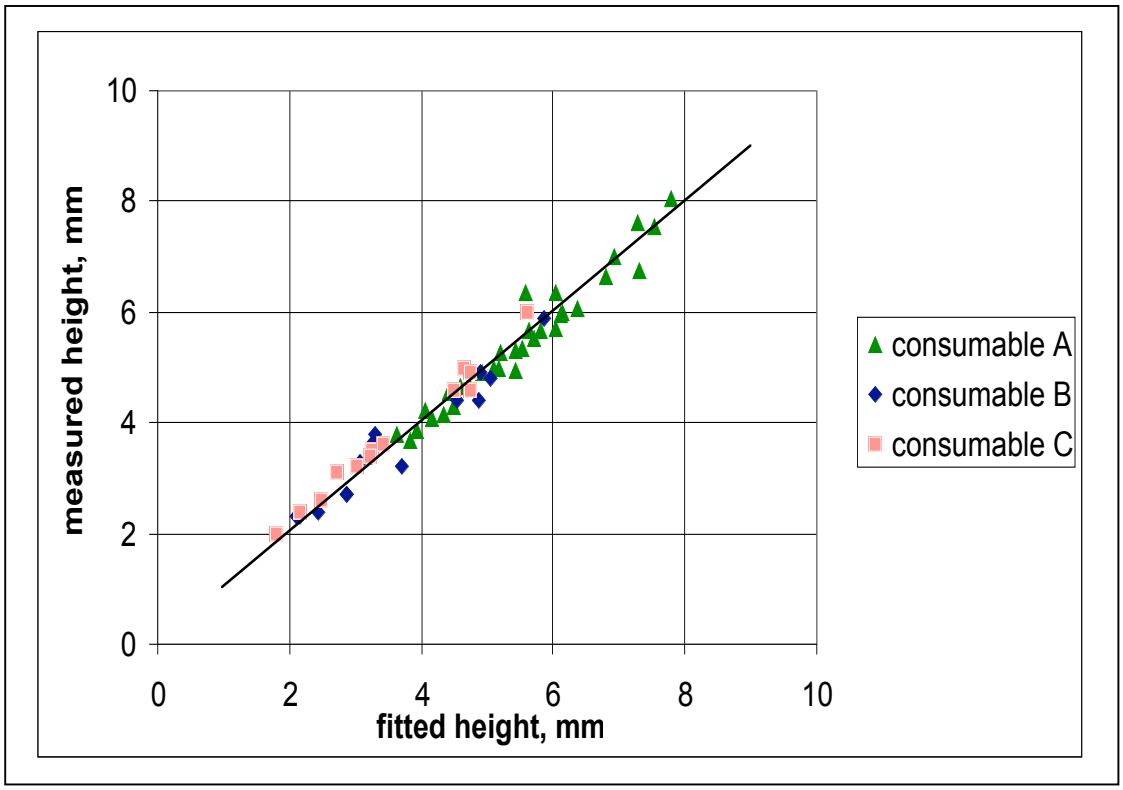

Figure 3.13: - Measured height vs fitted height with the empirical correction in equation 3.12. All samples were deposited with DCEP polarity.

3.5.2 The Effects of Work Distance and Preheat Temperature

The effects of work distance and preheat temperature on bead height are shown in Figures 3.14 and 3.15 respectively. The effect of work distance can be explained by the increase in deposition rate associated with increasing the work distance (see equation 2.4 – page 12). If all other parameters remain constant, the higher deposition rate will result in a higher bead. The effect of preheat temperature can be explained in terms of the associated increase in bead width. As the bead width increases the amount of deposited material has to be distributed across a wider bead, and a reduction in bead height will result.

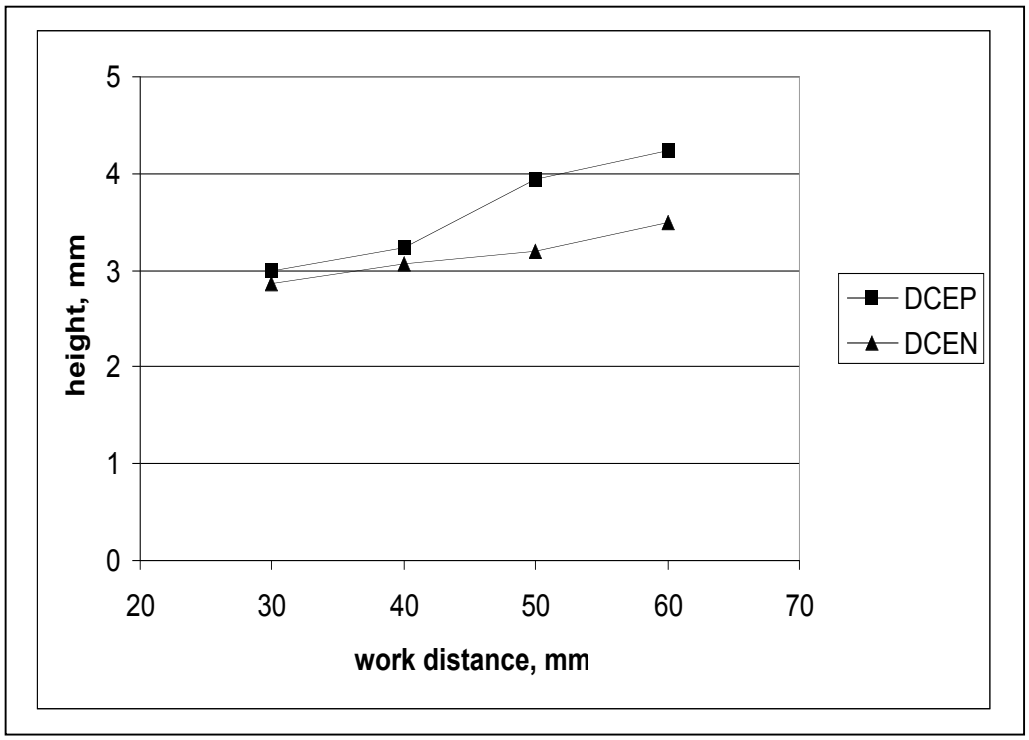

Figure 3.14: - The variation in bead height with work distance. All data points were obtained with consumable A. The base welding conditions were 31V, 300A, 350mm/min and no preheat.

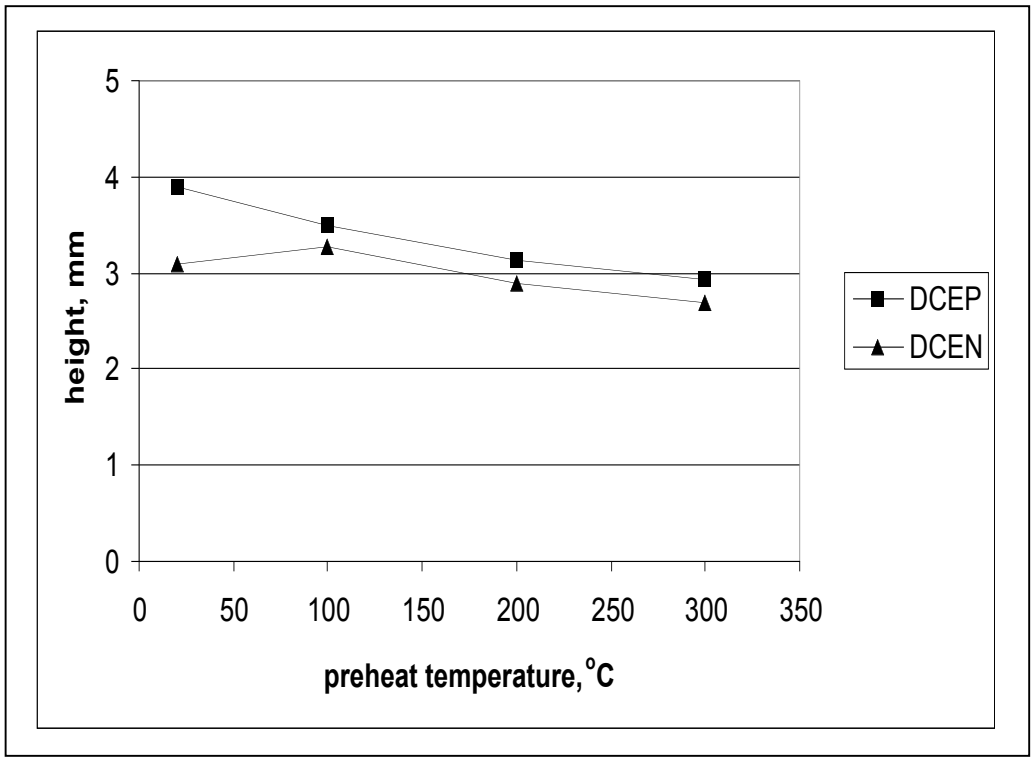

Figure 3.15: - The variation in bead height with preheat temperature. All data points were obtained with consumable A. The base welding conditions were 31V, 300A, 350mm/min and a 40mm work distance.

3.6 DILUTION OF SINGLE-BEAD DEPOSITS

3.6.1 The Bednarz-Deam Model (see Francis *et al.*,1998)

There have been few studies that investigate the effects of welding parameters on the dilution of single-bead deposits. A first-principles approach initiated by Deam (1996) and extended by Bednarz (1996) was discussed in Section 2.2.3. The model resulted in a general expression for the dilution of a single-bead deposit:

$$\frac{D_{sb}}{1 - D_{sb}} = \alpha \frac{VI}{W}\left(1 + \beta VIS\right) \quad \cdots\cdots\cdots (2.2) \qquad (\text{page } 10)$$

where D_{sb} is the dilution of a single-bead deposit and α and β are constant terms depending on the combination of welding consumable and substrate. Deposition rate data were measured for thirty-two samples deposited with consumable A and, for these samples, the dilution data have been fitted to the Bednarz-Deam model and are plotted in Figure 3.16. Measured values are plotted against fitted values.

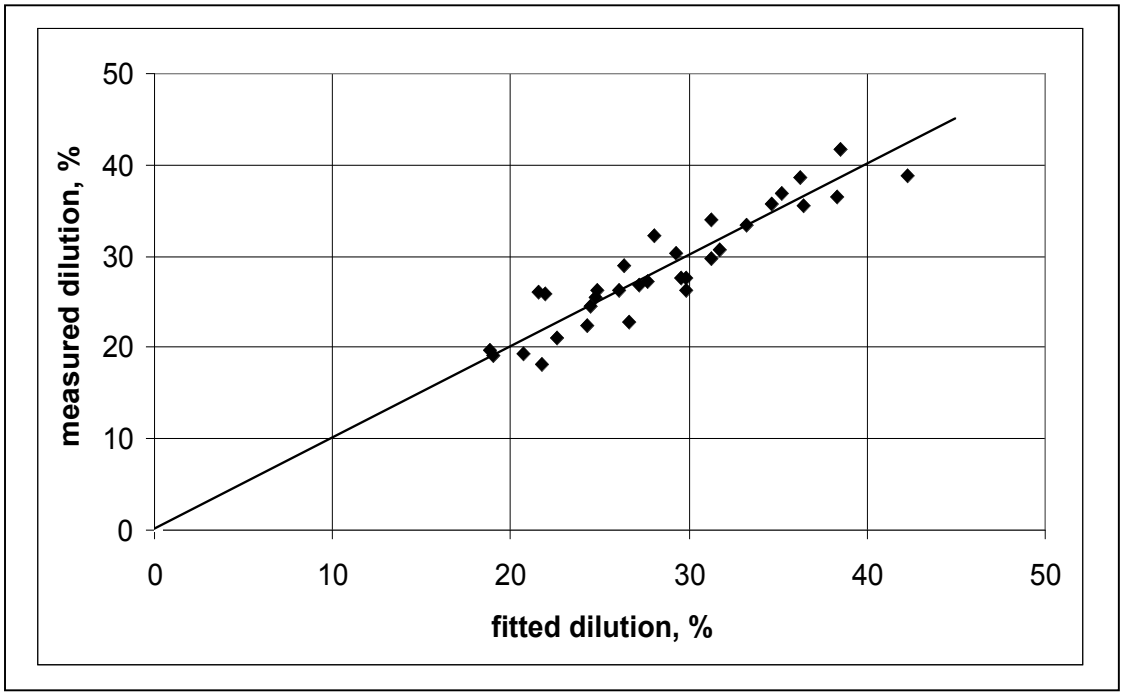

Figure 3.16: - Measured dilution data plotted against fitted values from the Bednarz-Deam model for single-bead dilution. The data were obtained from 32 single beads deposited with consumable A.

The model can be seen to describe the data with acceptable accuracy. An expression similar to equation 2.2 can be derived using equation 3.4 for bead width and equation 3.10 for the cross-sectional area of deposited material in a single-bead deposit. Christensen's model predicts that the fusion line for a single-bead deposit will be a semi-circle.

Thus, the cross-sectional area of melted substrate is:

$$A_{s(sb)} = \frac{1}{2} \cdot \frac{\pi w^2}{4} = \frac{\pi}{8} \left(\frac{C_1}{S} + C_2 VI \right)^2 \quad \cdots\cdots\cdots (3.14)$$

The cross-sectional area of deposited material is given by:

$$A_d = \frac{W}{\tilde{n} S} \quad (from\ equation\ 3.10)$$

If the area of melted substrate, $A_{s(sb)}$, is divided by the area of deposited material, A_d, it can be shown that:

$$\frac{D_{sb}}{1 - D_{sb}} = b_1 \frac{VI}{W} \left(\frac{b_2}{VIS} + 1 + b_3 VIS \right) \quad \cdots\cdots\cdots (3.15)$$

where b_1, b_2 and b_3 are constant terms relating to the particular combination of substrate and welding consumable. The derivation of equation 3.15 from equation 3.4 for bead width confirms that the Bednarz-Deam model and equation 3.4 are generally consistent with each other.

The single-bead dilution data shown in Figure 3.16 were fitted to equation 3.15. The fit did not improve, however, with the inclusion of the extra parameter.

3.6.2 The Effects of Work Distance and Preheat Temperature

The effects of work distance and preheat temperature on single-bead dilution are shown in Figures 3.17 and 3.18 respectively.

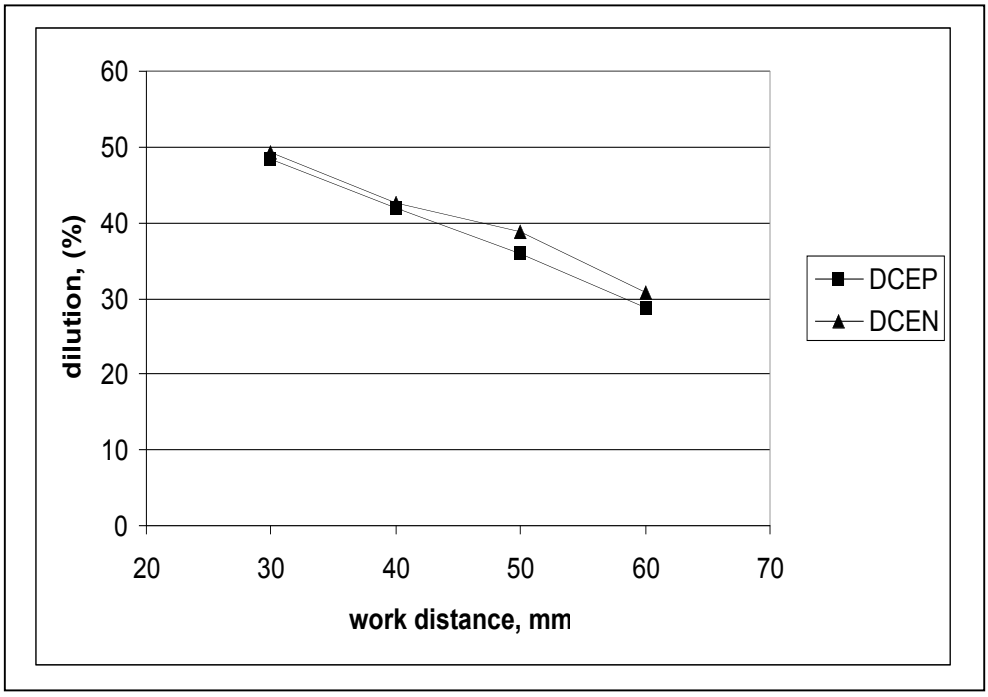

Figure 3.17: - The variation in single-bead dilution with work distance. All data points were obtained with consumable A. The base welding conditions were 31V, 300A, 350mm/min and no preheat.

Increases in work distance result in lower dilutions due to an increase in the deposition rate. However, Thorpe (1980) pointed out that the reduction in arc voltage associated with increasing the work distance may also contribute to reduced dilution. The reduction in arc voltage is caused by an increase in the voltage drop along the electrode between the contact tip and the arc. Increases in preheat temperature raise the dilution through increased melting of substrate material. Figure 3.18 shows, however, that the effect of preheat temperature is small for temperatures below 300^{o}C.

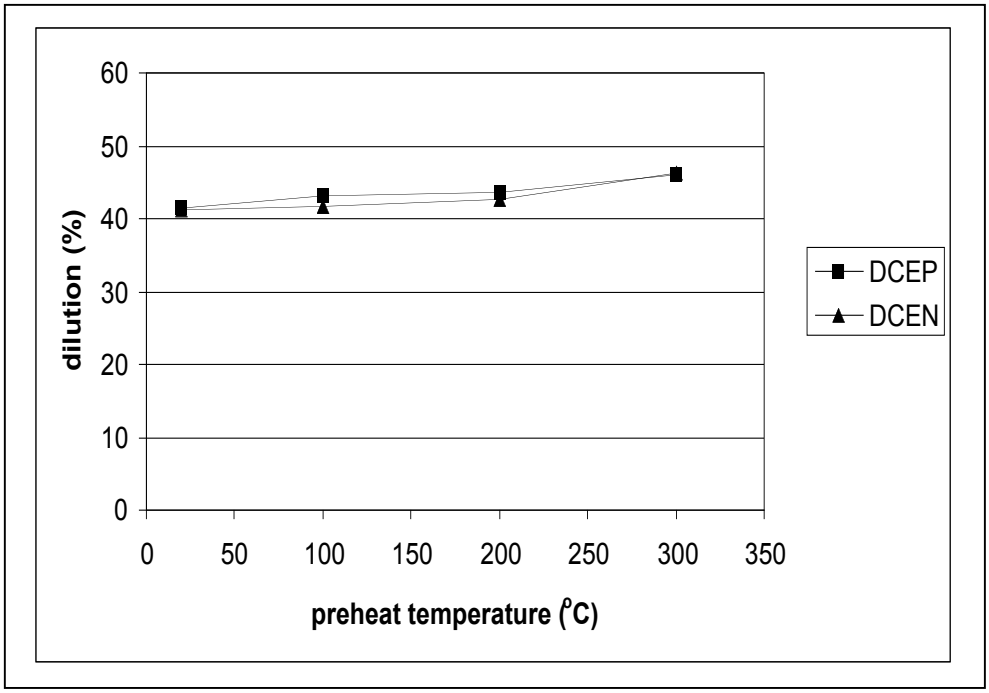

Figure 3.18: - The variation in single-bead dilution with preheat temperature. All data points were obtained with consumable A. The base welding conditions were 31V, 300A, 350mm/min and a 40mm work distance.

3.7 COMPOSITION OF SINGLE-BEAD DEPOSITS

If all of the welding consumable material that was melted was subsequently deposited as weld metal, the composition of a weld bead could be readily estimated from knowledge of the consumable composition and the dilution. Material is lost, however, in the process of welding through vaporisation, flux losses and other events such as spatter. That is to say, the *deposition efficiency* is less than 100%. The deposition efficiency, η_d, is defined as:

$$\eta_d = \frac{\textit{mass of weld metal deposited}}{\textit{mass of welding consumable melted}} \times 100\% \quad \cdots\cdots\cdots (3.16)$$

The deposition efficiencies calculated for consumables A and B are summarised in Table 3.2.

Consumable	Number of measurements	Mean deposition efficiency (%)	Standard Deviation (%)
A	56	95.1	3.8
B	15	97.6	1.4

Table 3.2: - A summary of the results of deposition efficiency measurements.

Given that the measured deposition efficiencies are high one might expect that it is possible to estimate the weld bead composition from the dilution and consumable composition. In order to test this hypothesis, combustion carbon and sulphur analyses were performed on eight weld beads deposited with consumable A. The beads were selected in such a way that they spanned a wide range of welding conditions and dilutions. The measured carbon concentrations were then compared with those predicted by assuming 100% deposition efficiency. The results are shown in Figure 3.19.

It can be seen that the predicted carbon concentrations are higher than the measured values. It is possible that this may be due to a disproportionate loss of carbon as the molten globules travel across the arc zone. An investigation of the factors leading to and affecting element loss is beyond the scope of this work. Consequently, the all-weld-metal composition will be used as a basis for all predictions of overlay composition.

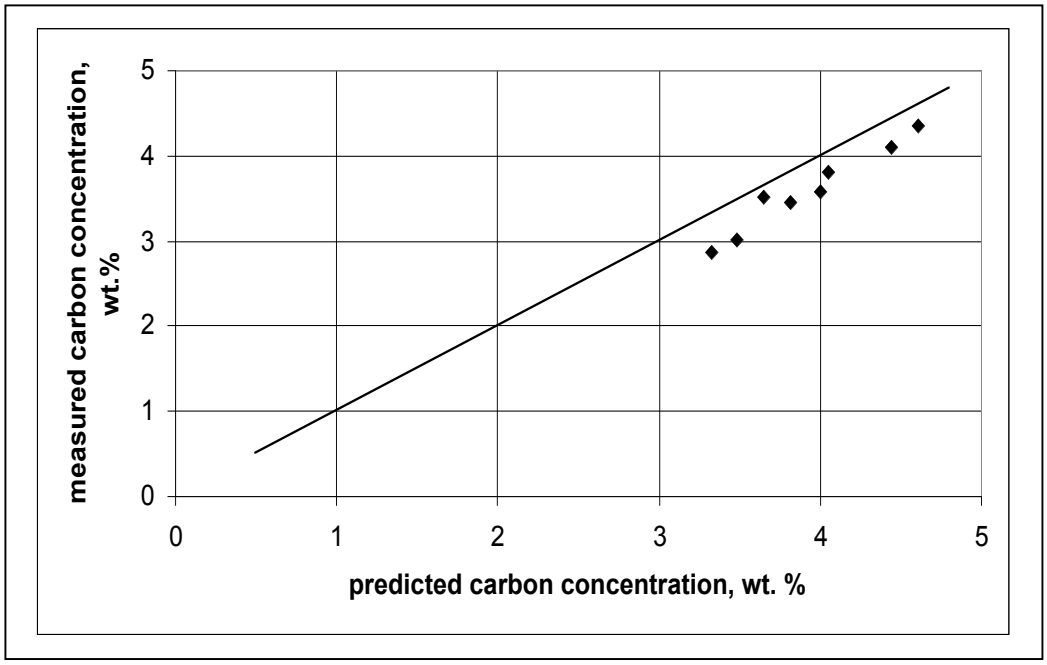

Figure 3.19: - A comparison of measured carbon concentrations for samples deposited with consumable A with those predicted by assuming 100% deposition efficiency.

3.8 CONCLUSIONS

A first-principles expression for bead width was developed. This expression suggests that the bead width increases with increasing welding current and welding voltage and decreases with increasing welding speed. These findings are consistent with those of the previous studies outlined in section 2.3.6.2. Equation 3.4 for the bead width was also found to be consistent with the Bednarz-Deam model for single-bead dilution.

An expression for predicting the height of single beads was also developed. It was based on the assumption that the profile of a single-bead deposit is a parabola. This assumption resulted in accurate predictions of bead height for low beads but, as the height of the beads increased, the predictions became increasingly inaccurate due to gravity-induced flow of the weld pool. However, the correlation between the predicted

bead heights and the measured values was strong and, with an empirical correction term, accurate predictions of bead height can be achieved.

Further work is required to develop a working expression for predicting the penetration of a single-bead deposit. However, the prediction of single-bead penetration is generally not essential in hardfacing operations. It is usually only necessary to predict the area of substrate that is melted in order to estimate the dilution. The first-principles model developed by Bednarz and Deam (see Francis *et al.*, 1998) was found to describe the single-bead dilution data in the current work with sufficient accuracy.

The deposition efficiencies of high chromium, high carbon welding consumables appear to fall in the range of 95 – 98 %, in agreement with the values quoted in the manufacturers' data sheets. The achievement of consistently high deposition efficiencies facilitates the prediction of deposition rate directly from the wire feed rate as set prior to welding. It should be mentioned that there are two methods of controlling deposition rate that find widespread use in the Australian hardfacing industry. The first, and most widely used, is to maintain constant settings for the welding current and work distance. Equation 2.4 (page 12) suggests that, under these circumstances, the deposition rate will remain constant. However, as a contact tip wears, the point at which electrical contact is made (between the tip and the welding consumable) may change. Thus wear of the contact tip may result in an effective change in work distance and hence a change in deposition rate. A more reliable method for controlling the deposition rate is to select and set the correct wire feed rate, accounting for the deposition efficiency. This approach is made easier if the deposition efficiencies are consistent and high.